1. Introduction

1.1 Problem Statement

There has been considerable success in detecting the supermassive black holes (SMBHs) in the Universe. They are the black holes (BH) with masses in the range 10^6 –$10^{9.5}$ M_s (10^6-$10^{9.5}$ times mass of the sun) , called so to distinguish them from the stellar mass black holes produced by the death of massive stars. There is no dearth of stellar-mass (1–15 M_s) black holes either; by some estimates there may be 10^7–10^9 in every galaxy. Black holes with masses in the range 10^2–10^4 M_s, appropriately called the intermediate-mass black holes (IMBHs), however remain a mystery. IMBHs have persistently evaded discovery in spite of considerable theoretical and observational efforts. Dense star clusters, such as globular clusters, have long been suspected as possible sites for the formation of IMBHs. The idea that some, if not all, globular clusters can host a central black hole actually preceedes the notion of the supermassive black holes, and more than thirty years ago attempts were made to discover them by their X-ray emission. Hunting for globular-cluster black holes was recognized as a task suited for HST's exquisite resolution which is needed to look close to a black hole. This idea was restimulated by the capability of Chandra X-ray Observatory to resolve sensitively the X-ray emission from the very centres of globular clusters; and recent detection of X-ray emission in the globular cluster G1 in M31 provided additional clue to the existence of an IMBH in this cluster. The growing evidence that some Galactic globular clusters could harbour central black holes, just as galaxies do, stimulates the searches and development of new methods for proving their existence.

1.2 Theoretical evidences of IMBH in GCs

- Runaway merger among the most massive stars in the globular cluster leads to the formation of an IMBH, provided that the core collapse proceeds faster than their main-sequence lifetime. For a globular cluster that evolves in the Galactic tidal field, the corresponding present-day half-mass relaxation time would have to be 10^8 years. Many of the Milky Way globular clusters have half-mass relaxation times in the range 10^8 –10^9 years, and some below 10^8 years.
- Another possible way for the formation of IMBHs in globular clusters is through the repeated merging of compact objects, if, for example, a single ~ 50 M_s BH were initially somewhere in the cluster, it would sink to the centre through dynamical friction, and slowly grow in mass through merging with stellar-mass black holes. Clusters with central densities >~ 10^5 pc^{-3} will have high enough encounter rates to produce 10^2 – 10^4 M_s BHs. In the Milky Way it would imply that roughly 40% of globulars could host such objects.

- Direct collapse of population III stars and subsequent growth by accretion, or the accretion of supernovae winds funneled by radiation drag exerted by stars on the interstellar medium, onto the cluster centre, forming the central massive object which eventually collapses to form an IMBH. While the first scenario does not require the host stellar system to be dense, the latter rules out the formation of the central BHs in most of the present-day galactic GCs on the basis of their insufficient total mass and/or central velocity dispersion.

1.3 Observational evidences for IMBH in Gcs

Several GCs were suggested to harbour IMBHs at their centres. The main evidence comes from the analysis of the central velocity dispersions of some GCs , and, in some cases, from the presence of a rotation in the core. Suggested upper limits of radio emission from low luminosity IMBHs in Gcs have led to upper estimates of the central BH mass in two nearby galactic GCs, 47 Tuc and NGC 6397. Detection of radio and X-ray from the GC G1 in M31 also supports the previous claims that it hosts a central BH. These IMBHs lie on the extrapolated $M_{\bullet}\sigma$ relation found for SMBHs in galactic nuclei, and this leads to a prediction of a central mass of ~ 10^3 M_s for a typical globular cluster having a velocity dispersion of the order of 10 km/s.

Despite the observational evidence of IMBH in GCs, there remains considerable debate about whether the reported excess of mass in the centres of GCs can be well modelled by a cluster of low-mass objects, such as white dwarfs (WD), neutron stars (NS)
or stellar-mass BHs, rather than an IMBH. None of the existing methods can distinguish between these two alternatives, mainly because the fitting procedure is relatively insensitive to the precise nature of the dark matter contained within the innermost region of the cluster. Detection of gravitational waves from an IMBH can be a potential method for resolving this argument, but for that the central IMBH has to be a binary and at final stages of coalescence. Gravitational microlensing of a background star by the central black hole, on the other hand, can in principle be a clear diagnostic tool as there is a significant difference in the lensing signatures of a single point-mass lens (a single IMBH), a binary lens, and, most importantly, of an ensemble of point-mass lenses (which would be the case if the central mass consisted of a conglomeration of low-mass objects). Thus the detection of a lensed signal in the centre of a GC can resolve the controversy about the nature of a central dark mass detected in some globulars and prove beyond doubt the existence of IMBH in GCs.

Paczynski was the first to suggest that lensing of stars in SMC or Galactic bulge can reveal compact objects in foreground GCs. However, it was found that the probability of such events is low and moreover such clusters are too few. It was also suggested to use GC stars as sources for halo lenses to distinguish between different galactic halo models. This would require monitoring each stars in a globular cluster or on average over all globular clusters about 60,000 stars. Both suggested methods would need very powerful telescopes with high resolution imaging.

1.4 Proposed Work

We propose to consider the microlensing events that are expected when globular cluster stars pass behind the central BH that acts as a lens, inducing amplification of light. We show here that by observing enough number of globular clusters there is a chance to prove the existence of an IMBH. This method removes some of the ambiguities usually present in the galactic microlensing events, because in GCs the location of both the lens and the source, and their velocities are well constrained.

2. Previous work: Aperture Photometry

Aperture photometry is the measurement of light which falls inside a particular aperture; usually, we mean a circular aperture of some fixed size.

In this photometry process, we first detect stars and then place an aperture over each star (fig 1) to measure total flux. These apertures are usually circular or elliptical in shape depending upon how degraded the PSF of that star is.

To estimate sky background place a second larger aperture around the first and measure the total flux in the area between the two.

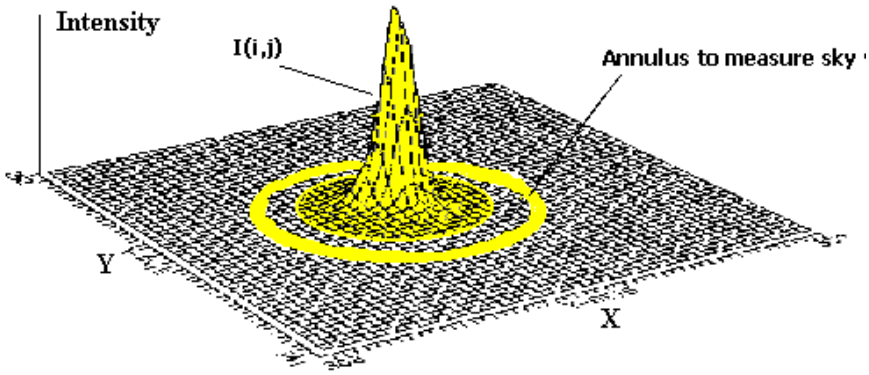

Fig 1

The major drawback of this method is that it doesn't work well with crowded fields as there is no space to place apertures on the stars as the stars are very congested fig 2).

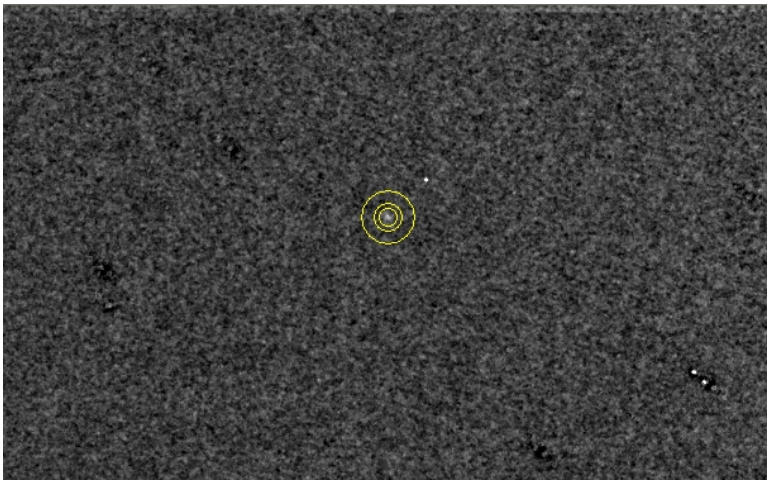

Fig 2

3. Globular Clusters and Microlensing

3.1 Introduction

Microlensing in the Galaxy is an intrinsically rare phenomenon. It happens to a couple of stars per million at any given time and this is why Galactic microlensing surveys are monitoring millions of stars in the densest fields of the sky: Galactic Center region and galaxies of the Local Group which are, at least partially, resolved into stars.

The price for reasonably high event rates is complicated systematics and limitations of the photometry in crowded fields. Overlapping stellar images make it hard to estimate the point spread function (PSF) and inevitably influence light centroid of the variables and number of detected sources. Over past few years it has become clear that the optical depth to microlensing cannot be reliably determined unless the effects of blending are considered. From the very beginning microlensing surveys are upgrading their photometry and detection techniques. In this area image subtraction is the most promising method, as it naturally removes numerous problems by eliminating multi-PSF fits. It is often referred to as the Difference Image Analysis (DIA) and we should probably settle on this terminology.

3.2 Overview of Photometric Method

Retrieving photometric information from images of crowded stellar fields is an important but at the same time a difficult task. The most serious complications are associated with overlapping stellar images. In such conditions it is virtually impossible to get a reliable background estimate, PSFs are ill defined, there are degeneracies in multi-parameter fits, and finally the centroids of the light for variable stars are influenced by neighboring stars. Any attempt to cross identify faint sources is bound to lead to a high confusion rate. For years, observers handled this problem using D O P HOT software, usually customized for a particular experiment. That package employs the traditional approach, that is the modeling of the heavily blended neighborhood for each star, and indeed, stands behind most of the important scientific results from microlensing so far. Various Attempts have been made for subtracting images of stellar fields over the past decade to eliminate fitting of multi-PSF models, however successful applications were usually limited to best quality data sets and focussed on one particular type of project. The demands encountered in microlensing surveys triggered new efforts in this area. Several groups are now using image subtraction algorithms based on convolution kernels derived from high signal to noise PSFs. The basic equation for this method would be:

$$Ker = FFT^{-1}\left(\frac{FFT(PSF\,1)}{FFT(PSF\,2)}\right)$$

A variation of this algorithm uses the above equation for the core of the PSF and supplements this with the analytic fit in the wings, where otherwise noise dominates the solution. This technique produced a number of results, but we believe it still suffers from some of the problems mentioned above. The derived kernel is obviously as weak as both PSFs, Fourier division is uncertain and difficult to control and the more crowding the worse it becomes.

Recently an algorithm has been proposed in which the final difference of two images of the same stellar field is nearly optimal (Alard and Lupton 1998). The basic idea is to work on full pixel distributions of both images and do the calculation in real space:

$$Im(x,y) = Ker(x,y;u,v) * Ref(u,v) + Bkg(x,y)$$

where Ref is a reference image, Ker is a convolution kernel, Bkg is a difference in background and Im is a program image. The above equation should be understood in the least squares sense and treats PSF gradients. To solve for the PSF matching kernel and background we minimize the squared differences between the images on both sides of the Eq. (2), summed over all pixels. It is assumed that most stars do not vary, and as a result, most pixels vary only slightly due to seeing variations. The problem is linear for kernels made of Gaussians with constant sigmas and modified by polynomials. For the full description of the algorithm see Alard (2000). Here we would like to emphasize that the knowledge of the PSF and background for individual images is not required and the method works better as the crowding increases, because in denser fields more pixels contain information about the PSF difference. It is very easy to impose flux conservation and the flux scale is automatically adjusted, so that the effects of variable atmospheric extinction and exposure time are taken out. Also, after correct subtraction the derived centroid of the variable object is unbiased by surrounding objects, as the variable part of the image is uncrowded. On the down side, the variables must be found before the actual measurement and the method requires some preliminary processing. Pixel grids of all images must be matched and images must be resampled. Preparation of the reference image to be subtracted from all the other frames takes some effort, and is an absolutely critical factor for the quality of the final result. The DIA method measures flux differences between the frames, also called the AC signal, as opposed to the DC signal, that is the total flux, given by most photometric tools. Intuitive arguments that measuring AC signal is inferior to having DC signal are a common misconception, at least in microlensing. It is certainly true that for some applications we need to know the total flux, not just the variable part of it. However, if we can be sure of our identification of the variable with an object seen on the reference frame, than we can calibrate the light curve on DC scale and the result will not be worse than using say D O P HOT on the reference image. It is often merely an illusion that we know what has varied in fields as crowded as Galactic bulge or globular clusters. Under such conditions caution should be exercised in the interpretation of the percentage flux variations. At a crowding level of one source per couple of beams, source confusion is as common

as correct identification. This is the essence of the blending problem in microlensing searches.

4. What is PSF (Point Spread Function)?

The **point spread function (PSF**) describes the response of an imaging system to a point source or a point object. A more general term for the PSF is a system's impulse response, the PSF being the impulse response of a focused optical system. The PSF in many contexts can be thought of as the extended blob in an image that represents an unresolved object. In functional terms it is the spatial domain version of the transfer function of the imaging system.

In observational astrometry the experimental determination of a PSF is often very straightforward due to the ample supply of point sources (stars or quarks). The form and source of the PSF may vary widely depending on the instrument and the context in which it is used.

For radio telescopes and diffraction-limited space telescopes the dominant terms in the PSF may be inferred from the configuration of the aperture in the Fourier domain. In practice there may be multiple terms contributed by the various components in a complex optical system. A complete description of the PSF will also include diffusion of light (or photo-electrons) in the detector, as well as tracking errors in the spacecraft or telescope.

For ground based optical telescopes, atmospheric turbulence (known as astronomical seeing) dominates the contribution to the PSF. In high-resolution ground-based imaging, the PSF is often found to vary with position in the image (an effect called anisoplanatism). In ground based adaptive optic systems the PSF is a combination of the aperture of the system with residual uncorrected atmospheric terms.

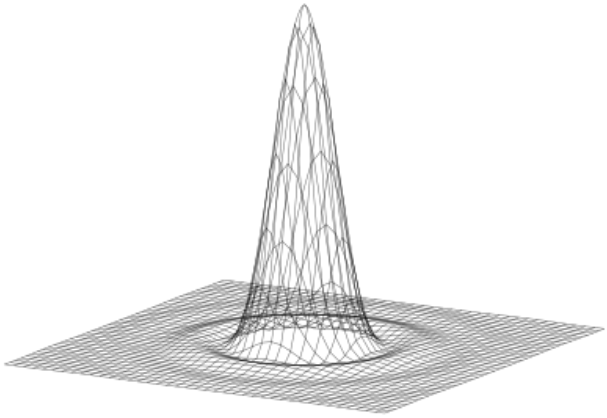

(Fig 3) PSF example

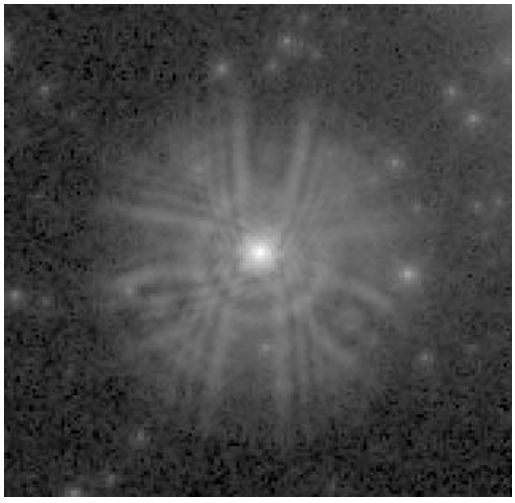

(Fig 4)The point spread function of Hubble Space Telescope's camera before corrections were applied to its optical system.

The major problem that we face in our work is distorted shape of the PSF in our astronomical image data. A perfect PSF should be round in shape whereas, the distorted PSF will smear out from its original shape.

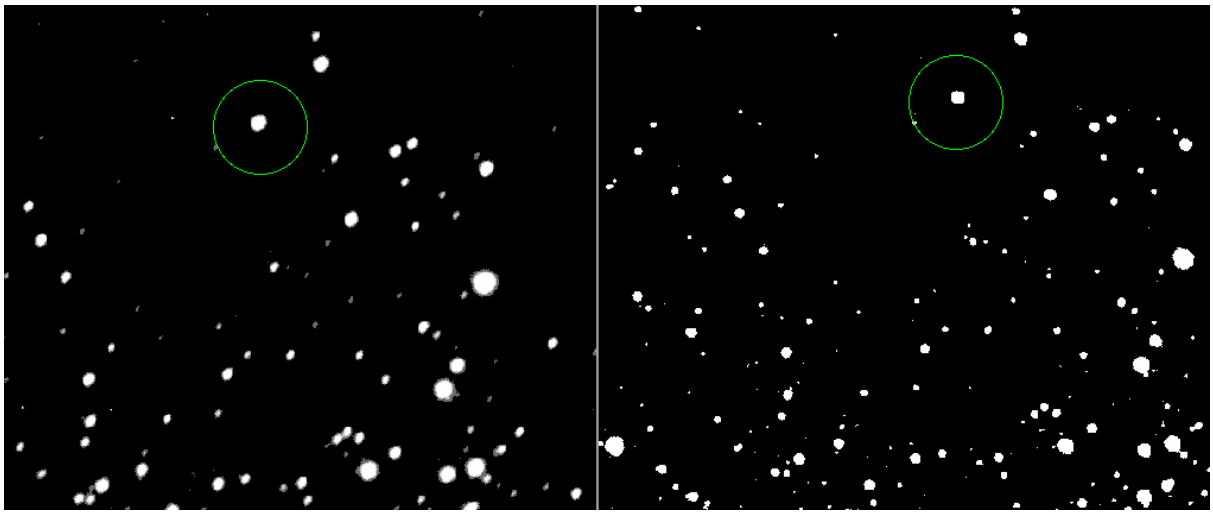

Fig 5(a) Bad PSF Fig 5(b) Good PSF

In fig 5 (a), for an example, we can see the shape of encircled object is not completely round. This can lead to the confusion that it is a binary system, which infact is not. As shown in the fig 5 (b).

Few of the most important reasons of why this phenomena takes place is:

1. Astronomical Seeing: Hinderance due to atmospheric refraction is considered as one of the most important reasons for PSF degradation

2. Turbulence due to wind: This affects the positioning of telescopes and can swipe through a region. It can result in trailing as shown in fig 6.

3. Adjustment of telescope lens: The incorrect adjustment of telesope lens will result in images with bad focus and also truncated.

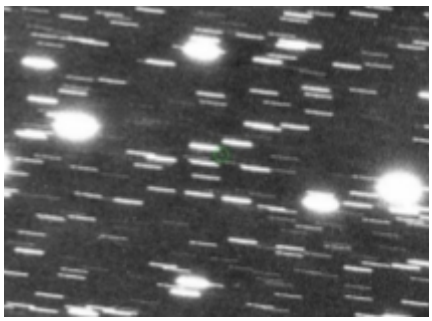

Fig 6: Trailing

5. Photometric Pipeline

We start with a general description of the data flow followed by more detailed descriptions of individual image processing algorithms in Sections 3.1 through 3.10.

To address the question of detectability of microlensing events in our sample of IMBH globular clusters, we take the case of the cluster M15, which was observed for feasibility in April 2008. The observations were carried out on the 2-m Himalayan Chandra Telescope (HCT) of the Indian Institute of Astrophysics, equipped with a 2K x 2K CCD, in V and I bands.

In the figure below, we show the central 2 x 2 arcmin square region of M15, observed in V-band for 50 sec. This exposure time was decided to avoid saturation of the core of the cluster in the image.

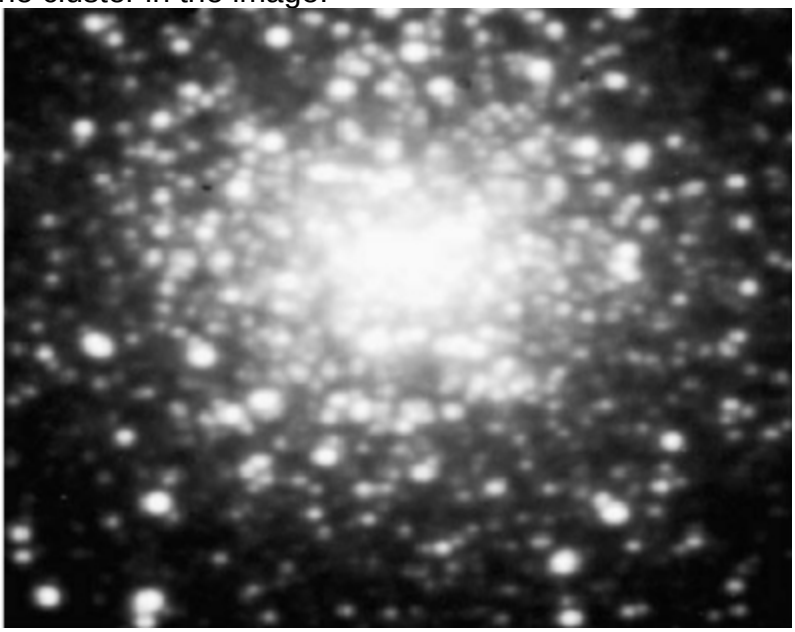

Fig 7: A globular Cluster

5.1 Selection of Frames for Construction of the Reference Image

For each field we need to select the best frames, which will be stacked together and used as a reference image in all subsequent subtractions. The properties of these images should be as uniform as possible. After 3 observing seasons OGLE collected typically 200–300 frames for a bulge field. Among those about 20 best seeing images also have low background and relative shifts in the range ¦ 75 pixels. Therefore we adopted 20 as the number of individual frames to be coadded. By definition we included the OGLE template image from D O P HOT pipeline (Udalski, Kubiak and Szyma´nski 1997) and used it as a coordinate reference to simplify cross identifications and transformations to celestial coordinates. All images were carefully inspected visually for possible background gradients, an occasional meteor,

and more importantly bad shape and spatial dependence of the PSF. About 25 images had to be reviewed before 20 could be satisfactorily included in the reference image. The seeing in the coadded image was typically 1.1 arcsec while the median for all of our data is 1.3 arcsec

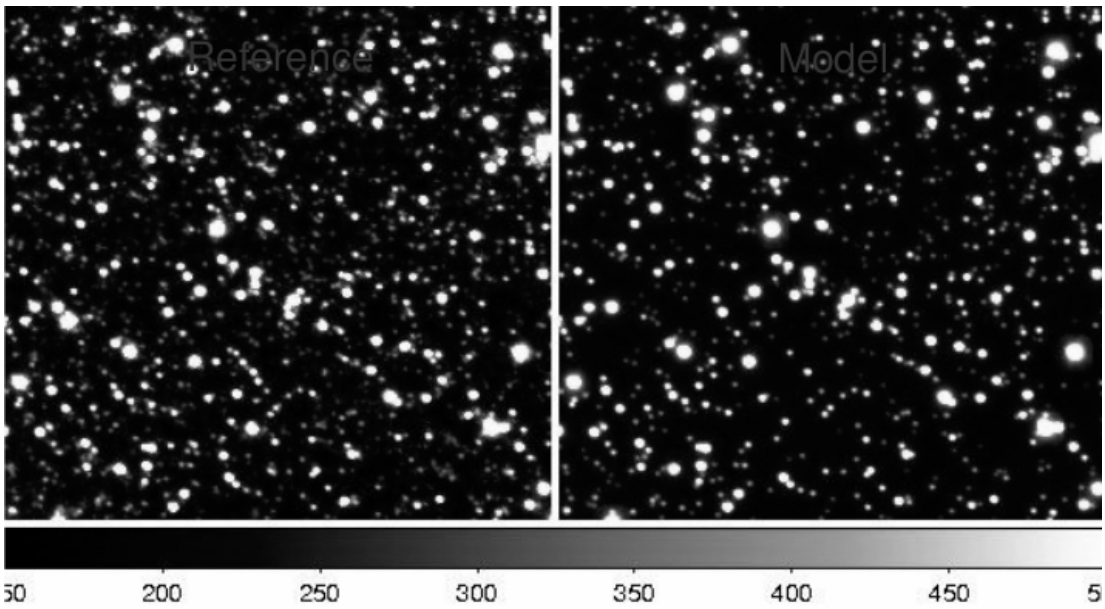

Fig 8: Reference Selection

5.2 Shifts between Frames

Before we can track the same piece of the sky in all frames we must first find a crude shift between each full frame and the coordinate template frame. This is best accomplished using a cross-correlation function

$$CRF(u,v)=\int f1(x,y)f2(x-u,y-v)\,dxdy$$

where `f 1, f 2` are images in question. To find the shift we just need to find the maximum of this function. For that purpose we used a central 2k x 4k piece of each frame. It may seem unnecessarily large, but in this way the software can tolerate very large shifts, and also there is more signal in the maximum we are looking for. Such large shifts were the case for several frames, which otherwise looked normal and had useful pixels in them. This is an adjustable parameter and could be changed for other applications.

Program CROSS subtracts first a median background estimate from both frames to avoid excessive baseline level for the resulting cross-correlation. Then the images are binned by a factor 16 in both directions to speed the whole process up. Fourier transforms of both images are taken and cross-correlation function is calculated as

$$FFT^{-1}\left(FFT(f1)\times\overline{FFT(f2)}\right)$$

where $\overline{FFT(f2)}$ indicates complex conjugate. The maximum of that function cannot be missed, especially in a crowded field! It is sufficient to take the brightest pixel to be the location of the maximum. Due to binning, the accuracy of this first guess is 16 pixels. The result will be refined to 1 pixel accuracy using the same method, but now on 128 ¢ 128 pixel central piece, adjusted for the initial guess and without binning. To save time CROSS can calculate FFT of the coordinate template frame once for the entire series of frames, and write all shifts to a single file.

5.3 Detection of stars and centroiding

For the purpose of detection of point sources the PSF can be approximated with a Gaussian of some typical width. We take the FWHM to be 2.5 pixels, about 1 arcsec. Program SFIND calculates the correlation coefficient with this approximate PSF model at each pixel by convolving with the lowered Gaussian filter and renormalizing with the model norm and local noise estimate. Convolved image has pixel values in [0,1] range. Local maxima of this image (defined by the brightest pixel in a square neighborhood of ±4 pixels) with the correlation coefficient above 0.7 are added to the list of candidate stars. Objects with saturated or dead pixels are ignored. In addition, the program outputs primitive aperture photometry using 1.5 pixel aperture radius and the median background estimate within an annulus between radii of 3.0 and 7.0 pixels. This photometry is used only to sort the sources in the order of increasing brightness. Detection threshold is set to provide ≈ 100 stars for fitting the coordinate transformation.

Centroids of detected stars are calculated using a 3 x 3 pixel neighborhood centered on the brightest pixel of a given star. To obtain the centroid in say X we integrate the flux in such neighborhood along Y to get 3 flux values at 3 integer values of X , and then find the location of the maximum of so defined parabola. We repeat this for Y . The scatter around the fit to the coordinate transformation between frames was used to asses the accuracy of the procedure. This simple algorithm, for our particular purpose, gave consistently better results than any other prescription we tried, e.g., fitting the position using a Gaussian approximation to the PSF.

5.4 Cross identification of stars betwen images

Cross identification of star lists for two images is done using a variation of the triangle method. It does not require the initial tie information, although our subframes are already corrected for the crude shift. Because of the nature of field distortions in driftscan imaging using OGLE telescope, the local residual shift with respect to the mean value for the entire 2k x 2k format can reach several pixels. The algorithm starts with the lists of all triangles
that can be formed from stars in both images. A triangle is defined by: the length of

the longest side, the ratio of the longest to shortest sides and the cosine of the angle between those sides. In so defined 3 dimensional space the program looks for close points using a combination of fractional and absolute tolerance levels. Because the cost of this method is $\sim n\times(n-1)\times(n-2)/6$ we can afford only 20–30 stars for the initial matching. These are selected to be the brightest stars in both lists, therefore the size of the subframe cannot be too large. In the case of a large format the slightest difference in the stellar magnitude corresponding to the saturation level, e.g., due to seeing variations, would shift the tip of the luminosity function by much more than 20–30 stars, making both lists exclusive. The initially matched list of ≈ 20 stars provides the linear fit to the coordinate transformation. It is sufficient for identification of all remaining stars needed in the final fit.

5.5 Resampling pixel grids

Program XYGRID takes the matched lists of coordinates for stars in two images and fits the full polynomial transformation between the two coordinate systems, which will enable the difference in the field distortions to be taken out. For our 540 x 156 pixel subframes we use 2nd order polynomials. The fit is cleaned by the iterative rejection of the points deviating by more than 3σ from the current best fit. Typical scatter in the matched positions is 0.06 pixels, consistent with our discussion of centroid errors in Section 4.2. It can be safely assumed that transformation is accurate to 0.1 pixels. Coefficients stored in a binary file are then used in program RESAMPLE to interpolate a given subframe. We use a bicubic spline interpolator. Pixels for which there is no information are given values which will be later recognized as saturated. At this point the images can be subtracted or coadded.

5.6 Image Coaddition

Preparation of the reference image requires stacking of frames, which is a relatively simple problem, since it does not require matching of the PSFs. If it were not for saturated pixels, bad columns and edge effects due to shifts, after resampling a simple mean value of each pixel would suffice. Things change if we want to save pixels which are bad only on some of the stacked images but otherwise have photometric information in them. We need to adjust for different background and scale of each frame, at least to the level when the effects of the patched defects in the final result are negligible.

Our simple algorithm for stacking was implemented in program MSTACK . We start with a series of 20 subframes. The first of them is a piece of the coordinate template and will also become the reference for background and scale. For each frame we prepare a histogram of pixel values. It is dominated by a broad sky peak at low values, followed by a much weaker wing due to stars, which extends all the way to the saturation level. In a crowded field the sky peak is heavily skewed by faint stars. We found that the simple fit for the scale and the background difference to all

the pixels in the image is very unreliable. The results are sufficiently accurate if we take the part of the peak inside its own FWHM and consider the flux such that 30% of the pixels in this trimmed distribution lies below. Then, for bright pixels we consider the ratio of their values in each image to the value in the first image (with the backgrounds subtracted). Assuming that the PSFs of all frames going into the reference image are similar, the variance weighted mean of the pixel by pixel ratios is an estimate of the scaling factor. The assumption is justified by the narrow range of the seeing allowed for the frames which were used in the construction of the reference image. To assure that the compared pixels belong to stars the minimum pixel level for this comparison is 300 counts above the upper boundary of the FWHM region of the sky peak. The results of these renormalizations are very good. It is impossible to tell which areas of the final frame have been recovered from minor bad spots. In particular the strip of 11 bad columns on the CCD chip of the OGLE camera disappears completely. It is important to realize that even if the backgrounds and scaling factors were in error, the pixel value of the final combined image would still be a linear function of the individual pixel levels (with the background offset). This matters only for noise estimates but in our case the reference image constructed here is treated as noiseless. Noise estimates later on are taken from individual frames.

The program has an option of using the median statistic instead of the mean. However it should not be used unless the seeings of the frames are matched. In this case even slight problems with the background levels and scalings will result in significant nonlinearity.

5.7 PSF Calculation

As mentioned before, the PSF is not required in order to obtain the PSF matching kernel and the difference frames. We determine the PSF solely for the purpose of the profile photometry on the difference images.

Substantial part of program GETPSF deals with the selection of good PSF stars. First the full list of candidate objects is selected at local maxima of the intensity, for which the highest pixel stands out by more than 2σ above the background, where is the photon noise estimate. A simplistic value of the flux is calculated using an aperture with 3.0 pixel radius. The frame is subdivided into 64 x 64 pixel boxes to ensure the uniform density of candidate PSF stars by selecting approximately the same number of stars in each box. We require about 100 PSF stars for the fit taken from bright end of the luminosity function. The peak value for a star is refined using parabolic fits in the 3 x 3 pixel area around the central pixel. The ratio of the background subtracted peak to the total flux in the object measures light concentration and is required to be less than 20% for stars. For most cosmic rays this parameter is much larger. The sample of well behaved stars is cleaned of misshapen objects, e.g., cosmic rays and very tight blends, using sigma clipping on the distribution of light concentrations. Finally, candidates for the fit are checked for close neighbors. The star is rejected from the fit, if in the area ±3 pixels around the peak there is another local maximum at least 2σ above the background and brighter than 0 15 x r x f_{peak} , where r is the distance in pixels and f_{peak} is the peak flux of the

candidate star. With typical FWHM seeing values of around 3 pixels, this eliminates stars which have fluxes significantly contaminated due to crowding.

The PSF model consists of two Gaussians, one for the core and one a factor of 1.83 wider for the wings, each multiplied by a 3rd order polynomial. Both Gaussians are elliptical. The position angle of the major axis and ellipticity can vary but remain the same for the core and wing components. Spatial variability is modeled by allowing each of the local polynomial coefficients to be a function of X Y coordinates across the format, also a polynomial, but this time of the 2nd order.

The first guess for the shape of the Gaussians is taken to be circularly symmetric and the initial FWHM of the core component is 3.0 pixels. The linear and nonlinear parts of the fit are separated. The shape of the Gaussian and its centering are nonlinear parameters and they are adjusted iteratively since the required correction is often minute, certainly for our data. Also, the individual amplitudes of stars must be taken out before the fit to generic PSF parameters. Therefore in each iteration we first solve the linear problem for all polynomial coefficients, then we update the shape of the Gaussian using moments of the light distribution of the current fit and finally we correct centroids of fitted objects with linearized least squares and recalculate the norm of each star. To avoid any potential instability the first few iterations are done with spatial variability turned off and then the full fit can be safely completed. In our case only 2 iterations are required at each stage.

PSF coefficients are stored in a binary file for later use in detection of variables and profile photometry on difference images.

5.8 Subtraction

The goal at this stage of the data processing is to find the best PSF matching kernel and subtract the reference image from all the remaining images. It takes a series of frames resampled onto a common pixel grid of the reference frame. We did not use the capability for external masking of unwanted pixels, because the internal rejection algorithms gave us satisfactory results.

The heart of the method is the choice of the kernel decomposition: 3 Gaussians of constant widths multiplied by polynomials. The kernel in this form is linear in the parameters, making the solution of Eq. (2) simply a big least squares problem. We used Gaussians with sigmas σ=0.78 , 1.35, and 2.34 pixels modified by 2D polynomials of orders n = 4, 3, and 2 respectively. The above parameters previously gave us good results for ground based data sampled near the Nyquist frequency. Convolutions are performed directly, i.e., in real space, using a 15 x 15 pixel rasters for the kernel components. This is considerably faster than Fourier calculation in the case of a large difference between the spatial scales of the functions to be convolved. Spatial variability is introduced by allowing each of the local kernel coefficients to be a function of X Y , again a polynomial, to keep things linear. The spatially variable problem quickly grows, the number of coefficients is $(n_{spatial}+1)\times(n_{spatial}+2)/2$ times larger than in the case of a constant kernel and can exceed 100 in normal applications, still affordable in terms of the S/N ratio given the

enormous number of pixels. We used second order spatial dependence, $n_{spatial}=2$. The program also fits the difference in backgrounds between the images. A first order polynomial was used for that purpose.

The first step is convolving a reference image with each piece of the kernel to form a set of images, which can be viewed as the basis vectors. Solving Eq. (2) means finding a linear combination of these basis vectors that closest reproduces the light distribution of the frame to be differenced. Because of the computing time requirements spatial variability is handled by subdividing the fitted area into a number of square domains, sufficiently small so that the PSF variability can be ignored inside a single domain. Local kernel coefficients at the domain center are adopted for the entire domain, here 23 x 23 pixels. Some pixels are better left unused, e.g., those which vary because they belong to variable stars, not due to seeing. Also one should avoid fitting large areas dominated by the background, where all the structure is dominated by noise and the resulting kernel will display the large amplitude, high frequency oscillations. In crowded fields this is never a problem. Due to the finite width of the kernel for some pixels the value of the convolution cannot be determined. Pixels near the edges of the image or near unusable pixels are rejected with the safety margin of 7 pixels (half width of the kernel) for convolutions and 2 pixels for other images. Two choices of the domain patterns are available: uniformly distributed domains or centered on bright stars. By trial and error we determined that the kernel fits are best in the second mode with 20 ¢ 10 individual domains spread over the area of a subframe. Once the appropriate domains in the basis images have been selected, we obtain the first guess for the solution. To solve the Eq. (2) we used LU decomposition from numerical recipes throughout our programs. The initial solution is cleaned with sigma clipping of individual pixels within domains and clipping of the entire distribution of whole domains using their χ^2 per pixel values. We require that after sigma clipping at least 75% of the domain area must be acceptable for the domain to enter the final solution. Also at least 40% of the total fitted area must be left in the fit and the final χ^2 per pixel must be less than 8.0 for the program to declare a successful subtraction. If this is the case, the reference image is convolved with the best fit kernel and subtracted from the program subframe. Otherwise the subframe is rejected and flagged as such. At the end the code writes the difference frames and kernel coefficients to binary files.

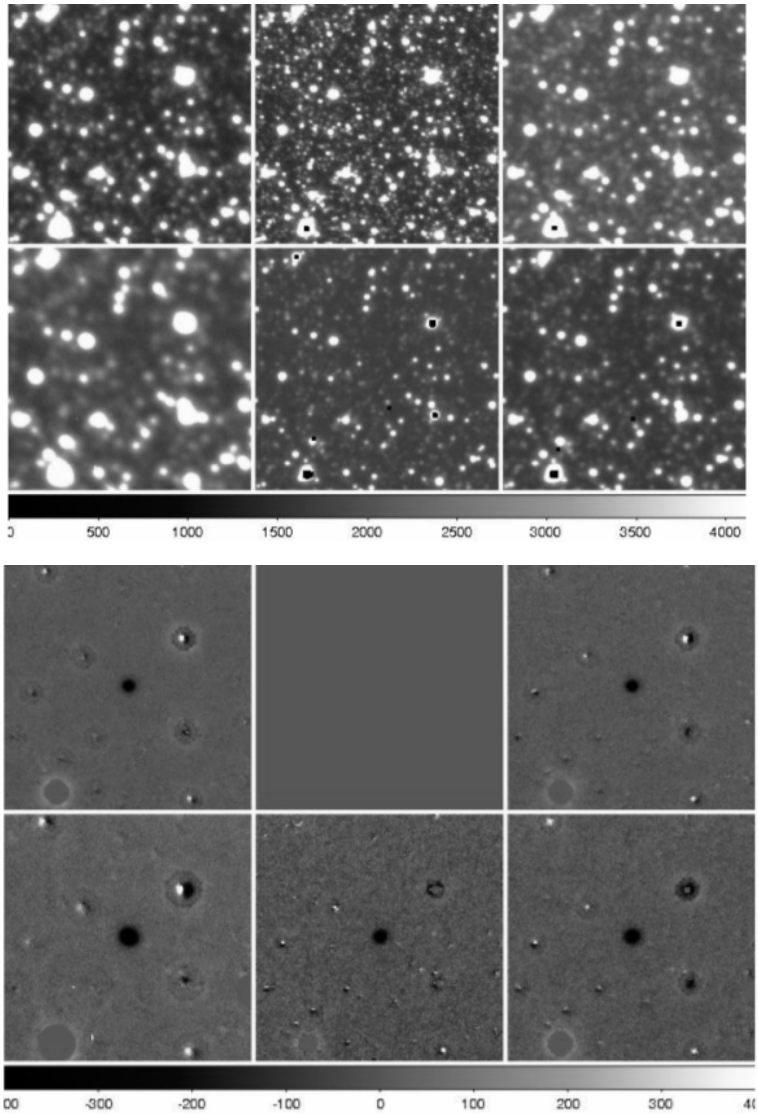

Fig 9 (Above) and Fig 10 (Below): Set of images before and after subtraction.

5.9 Finding variables and Centroiding

We decided to detect variable objects using some preliminary variability measures based on the entire series of difference images for a given field, and make final measurements only for those candidates. We also avoided strong assumptions about the type of flux variations to be extracted. The main idea is to encode all interesting variability of several basic types in a corresponding number of “variability images”, find variables in these frames and calculate their centroids. A single value for the centroid for each variable is calculated using the entire series of difference frames, which eliminates the need for cross identification of variables between images and enables the measuring of photometric points for frames on which the difference signal for a given variable has not been detected. This way our databases

contain only the light curves for candidate variables, non-variable stars will not be included. Our algorithm for finding variables may not seem especially natural, but it is the most efficient we could find in the sense that it recovers practically all stars which appear variable upon visual inspection of the difference frames, and does not return too many spurious detections. In fact about 80% of the 4597 candidate variables in the database for SC1 bulge field could be classified as one of the known types of the periodic variables or had significant night-to-night correlations in their light curves, which are a strong indicator of real variability (Mizerski and Bejger, private communication). The remaining objects are either non-variable stars which passed our selection cuts, or ghost variables caused by various undetected problems, e.g., the telescope tracking errors or cosmic rays. We deliberately admit some noise background in the catalog to provide the testing ground for new automated variability classification schemes.

Program GETVAR starts by rejecting some fraction of the frames with the worst seeing, in our case 10%. It also uses a conservative value for the noise estimate, 1.6 times photon noise. This factor matches the average quality of subtraction measured by χ^2 per pixel and is a correct scaling for red clump giants, bright stars which dominate the solution of the main equation for the PSF matching kernel (Eq. 2). For faint stars this is an overestimate, as shown in Section 4.1, but the detailed noise properties of the data were not known at the time when parameter values had to be selected.

In the next step we consider individual light curves in the 3 x 3 pixels square aperture centered on every pixel. This corresponds to smoothing of all difference frames with the 3 pixels wide mean filter before examining pixel light curves. Some points are rejected for saturated and dead pixels and we require that at least 50% of the measurements remain in the cleaned light curve. For each pixel light curve we take the median flux to be the baseline flux and analyze the ratios of the departures from this base level to their noise estimates. The specific numbers we quote here are all adjustable parameters of the program. To include periodic and quasi periodic variables which vary continuously, as well as eclipsing binaries and other transient phenomena like flares and microlensing, we have two channels for selecting variable pixels. The pixel is declared as variable if one of the two conditions are met:

1. there are at least 3 consecutive points departing at least 3σ from the baseline in the same direction (up or down), or
2. there are at least 10 points total departing at least 4σ from the baseline in the same direction not necessarily consecutive.

In the next step we label variable pixels according to the ratio of the number of the deviating points from the above cut which depart upwards to the number of points departing downwards. If the ratio is between 0.5 and 2.0 we fill a corresponding pixel of the variability image for “continuous” variables. Otherwise we fill the pixel of the image for “transients”. As the measure of pixel variability we adopt $D = \sum_i |F_i - F_0|$ where F_i is the flux and F_0 is baseline flux. For “continuous” variables the pixel value

$$D = \sum_i (D_{up} + D_{down}) / (n_{up} + n_{down})$$

in the variability image will be: where n is the number of points high or low with respect to F_0 . For "transients" variability image will contain: D_{up} / n_{up} or D_{down} / n_{down} depending whether $n_{up} \geq n_{down}$ or $n_{up} < n_{down}$ respectively.

As mentioned before we determine the centroid of a variable only once using entire series of difference images. The program takes 9 x 9 pixel rasters centered on each variable from frames on which the difference between the measured flux and the template flux was at least 3σ. The absolute values of these rasters are subsequently weighted by their signal to noise and coadded to accumulate as much signal in the peak as possible. Using a 3 x 3 neighborhood of this peak and parabolic fit we calculate the centroid in exactly the same way as for regular frames.

Cross identification of variables from "continuous" and "transient" channels is done because some of them can in principle appear in both lists. Variables closer than 2.0 pixels are treated as one and are given the value of variability type 11. "Transients" are type 1 and "continuous variables" are type 10. Currently these are all variability types included, but the extension to other types should be straight-forward. One interesting example to consider in the future might be a single high point, which would filter moving objects.

The final step is simple PSF and aperture photometry on the reference image at the location of the variable. It must be emphasized that this photometry does not attempt any modeling of the surrounding stars and therefore for faint and/or blended variables it can be severely contaminated by the neighbors. This information provides only a quick check of how much flux there is in the template image at the location of the variable, because the actual light curve contains only the difference signal. We also set a crowding flag equal to 1 if there is a pixel brighter than 0 15 x r x f in the ±4 pixels neighborhood, where r is the distance (in pixels) and f is the flux of the central pixel of the variable on the reference image. Given that in the reference images the FWHM of the seeing disk is typically less than 3 pixels, for an object with the crowding flag set to 0 (uncrowded) it will be likely that less than 10% of the flux within its PSF belongs to the neighboring stars.

5.10 Photometry

We perform both profile and aperture photometry in our difference images, keeping the centroid fixed. Aperture photometry and its noise are given by Eqs. (5) through (7).

$$a_{ap} = \sum_i^{n<r_{ap}} f_i$$

$$\sigma_{ap} = \sqrt{\sum_i \sigma_i^2}$$

$$\sigma_i^2 = f_{i,0} / G$$

where f_i is the difference flux in pixel i, $f_{i,0}$ is the actual pixel flux including background

and before subtraction of the reference image, the sum is over pixels with centers withing the aperature radius r_{ap} from the centroid. G is the gain in e^-/ADU.

Profile photomety comes down to a 1 parameter fit for the amplitude with

$$\chi^2 = \sum_{i}^{r_i < r_{fit}} (a_{psf} P_i - f_i)^2 / \sigma_i^2$$

P_i at pixel i is the value of the PSF profile centered on the variable and the sum is within the fitting radius r_{fit} around the centroid. The best fit is given by:

$$a_{psf} = \frac{\sum_i (f_i P_i / \sigma_i^2)}{\sum_i (P_i^2 / \sigma_i^2)}$$

$$\sigma_{psf} = \frac{1}{\sqrt{\sum_i (P_i^2 / \sigma_i^2)}}$$

Obviously the PSF photometry gives optimal noise and allows the meaningful renormalization for the rejected saturated and dead pixels. Progra, PHOTO takes a series of difference frames, resampled frames before the subtracted for noise estimates, coefficients of spatially variable PSF matching kernel for each subframe and finally the coefficients of the PSF for the reference frame. By convolving local kernel and reference PSF for each subframe it constructs a PSF profile at the position of each variable and calculates amplitude a_{ap} and a_{psf} with corresponding errors σ_{ap} and σ_{psf} , which involves little more than simple sums over pixels. We used $r_{ap} = r_{fit} = 3.0$ pixels. Whenever there is no information, PHOT will put requested error codes to keep the record of such gaps. The final light curves are stored in a binary file. Records for all epochs for a given variable must be written before the next light curve can be stored. The total number of 40 byte records is equal to $n_{variable} \times n_{epochs}$. The time vector is the same for all stars and therefore it is more efficient in terms of storage to keep it separately in a short ASCII file. All fields of the record are 4 byte FLOAT numbers except for the last one, which is a 4 byte INTEGER; the most significant byte is stored first. The format of the binary record is the following:

1. flux – profile photomerty
2. flux error – profile photometry
3. flux – aperture photometry
4. flux error – aperture photometry
5. background
6. χ^2 per pixel for the PSF fit
7. correlation coefficient with the PSF
8. χ^2 per pixel of subtraction of entire corresponding subframe
9. FWHM of the PSF profile

10. number of bad pixels within the fitting radius

As in the case of the catalog the results for SCI field in public domain are available in ASCII format.

6. Observation

6.1 Selection of targets and observational strategy

Ideally, we would monitor all Galactic globular clusters. However, in practice it is a very difficult task. Even in our selected candidate list, it is found that the optical depth varies considerably. Besides, the tentative results shows, it might be useless to look for diffuse, faint and distant clusters. Moreover, in PCC clusters, if we take into account the mass segregation effect, and/or a mass distribution law more concentrated towards the centre, a $r^{-7/4}$ profile, the lensing rate increases. For example, for nearby 47 Tuc, NGC 6397 and NGC 6752 it would nearly double (18.6×10^{-6} and 2.6×10^{-6}, respectively).

Assuming the threshold optical depth for choosing the observational targets as 1×10^{-6}, we plot the dependence of the optical depth on core radius and central density. In order to have larger optical depth, a cluster has to have either large core radius and/or large central density rather than the core radius. Dense compact clusters are potentially better targets for monitoring programs aimed ar detecting IMBHs.

6.2 Prospects for detection

The requirements of a traditional absolute photometry argue that cluster ML observations shall be carried with a large telescope with subarcsecond seeing. However, the cores of most GCs are not resolved even with an HST and, besides, it is not necessary to monitor every star in a globular cluster; the differential imaging analysis (DIA) takes the practice of crowded field photometry to its extreme limit. DIA is sensitive to ML events even when the source star is too faint to be detected at the baseline. We do not expect to be able to resolve the source star in the crowded centres of globular clusters, but with a careful application of DIA we do expect to be able to detect the star during any suitably bright outburst episode

It is interesting to mention that, inevitable in the case of a GC microlensing effects of blending (the contribution to the observed ML light curve from other unassociated sources) could be used to learn more about the lensing event than would be possible if there were no blending. The rate of lensing can actually increase in the crowded fields (Di Stefano and Esin, 1995), because there are many possible lensing events associated with the low-mass stars in the

resolution cone of the telescope, instead of just one event associated with lensing of a single isolated star. For example, observing a region at μ_v 19 ^{mag}/1 arcsec ^{2} increases event probability by more than a factor of 10 compared to observing in a 14.5 mag region. Blending plays a significant role in making the lensing of lowest mass stars either more or less observable. Blending also reduces the duration of events as well, thus it would reduce somewhat the rather long baseline of observations necessary for central BH cluster microlensing

6.3 Identifying genuine ML events

One major difficulty in identifying genuine lensing events is contamination by variable stars (periodic variables, cataclysmic variables (CVs) such as classical novae and dwarf novae (DN)). However, globular clusters contain very few CVs and especially erupting CVs, which may mimic microlensing events. The total number as of 2007 was 12 DN in seven galactic globular clusters. The light curves of variable stars are much different from symmetric and achromatic Paczynski curves shown by lensing events Paczynski. Most stellar variables are normally bluer when they are at maximum flux. Thus by carrying out two-colour photometry in V and I bands, and by fitting the observed light curves to a Paczynski curve, variable stellar sources, that may cause contamination, can be removed. The estimated timescales of GC ML events are of the order of a year, whereas most of the variable stars in GCs have short periods (<100 days). Therefore, by analyzing the observed candidate light curves for the abovementioned properties, contaminating stellar variables can be efficiently removed from genuine ML events.

Self-lensing events may present a challenge due to its higher event rate. However, as far as competition between IMBH and self-lensing is concerned, the probabilities are very different. The probability of self-lensing does not depend as drastically on the radial distance as the IMBH lensing. If we consider a tube through the GC centre with radius = core radius (which is much more than the radius of an IMBH influence), the ratio of self-lensing probabilities would roughly go as $\tau_{core}/\tau_{allcluster} \succ r_{core}/r_{allcluster}$, which shows immediately how negligible it would be in the centre. Stars behind the cluster centre cannot contribute to self-lensing optical depth; any self-lensing event there would only contribute to the photometric noise. Also, contrary to the tentative conclusion on the choice of GC to look for IMBH lensing, the less centrally-concentrated,

loose and diffuse clusters are more favoured for self-lensing search, and such clusters are excluded from our current proposal. In addition, self-lensing time scales are of the order of days, compared to the year-long time scales of GC ML events.

GC stars can also be affected by microlensing due to compact matter in the Milky Way not associated to a globular cluster. However, in such cases, the lens transverse velocity is set to that of the Galactic disk rotation, v ≈ 220 km/s, which would give the typical timescale of event ~20–30 days. Such events too will occupy a separate region
on the amplitude-duration diagram and again can be easily distinguished from long-duration ML events and eliminated.

7. Conclusion

Determining whether globular clusters contain IMBHs is a key problem in astronomy. IMBHs may contribute as much as $\Omega \approx 0.02$ to the cosmic baryon budget. Their cosmic mass density could exceed that of supermassive BHs ($\Omega \approx 10^{-5.7}$) and the observations do not even rule out that they may account for all the baryonic dark matter in the Universe ($\Omega \approx 10^{-1.7}$). They also may have profound influence on the evolution and survival of globular clusters. In this paper, we have outlined the novel technique for using microlensing to detect IMBH in the centres of GCs. We suggest that dense and bright GCs are better suited to search for IMBH than diffuse and low-luminosity GCs. The OH, BD and SC clusters are the most likely ones.

Our suggested monitoring programme of observing ~100 clusters over a 10 year baseline with a time resolution of one observation per month will permit detection of one ML event. Such a monitoring programme is feasible on any dedicated 2 m class telescope involved solely in monitoring astronomical sources. All the potential contaminants to this lensing signal can be easily identified and eliminated from the true ML events.

8. References

1. “Detection of IMBHs from microlensing in globular clusters” M. Safonova , C.S. Stalin
2. “Difference Image Analysis of the OGLE-II Bulge Data. I. The Method” P. R. Wozniak
3. “Image subtraction using a space-varying kernel” C. Alard
4. “A Method for Optimal Image Subtraction” C. Alard, R. H. Lupton
5. “StarFinder: an IDL GUI based code to analyze crowded fields with isoplanatic correcting PSF fitting” E. Diolaiti, O. Bendinelli, D. Bonaccini, L. M. Close, D. G. Currie and G. Parmeggiani
6. “Detection of Variable Stars in the Open Cluster M11 Using Difference Image Analysis Pipeline” Chung-Uk Lee, Jae-Rim Koo , Seung-Lee Kim, Jae Woo Lee, Byeong-Gon Park and Cheongho Han
7. “From raw images to lightcurves: how to make sense of your data” Yiannis Tsapras